Laser controlled charge-transfer reaction at low temperatures

Alexander Petrov, Constantinos Makrides, and Svetlana Kotochigova

Citation: The Journal of Chemical Physics **146**, 084304 (2017); doi: 10.1063/1.4976972
View online: http://dx.doi.org/10.1063/1.4976972
View Table of Contents: http://aip.scitation.org/toc/jcp/146/8
Published by the American Institute of Physics

Laser controlled charge-transfer reaction at low temperatures

Alexander Petrov,[1,2] Constantinos Makrides,[1] and Svetlana Kotochigova[1]
[1]*Department of Physics, Temple University, Philadelphia, Pennsylvania 19122, USA*
[2]*NRC Kurchatov Institute PNPI, Gatchina, Leningrad District 188300, Russia and Division of Quantum Mechanics, St. Petersburg State University, University Embankment 7-9, St. Petersburg 199034, Russia*

(Received 31 October 2016; accepted 6 February 2017; published online 24 February 2017)

We study the low-temperature charge transfer reaction between a neutral atom and an ion under the influence of near-resonant laser light. By setting up a multi-channel model with field-dressed states, we demonstrate that the reaction rate coefficient can be enhanced by several orders of magnitude with laser intensities of 10^6 W/cm^2 or larger. In addition, depending on laser frequency, one can induce a significant enhancement or suppression of the charge-exchange rate coefficient. For our intensities, multi-photon processes are not important. *Published by AIP Publishing.* [http://dx.doi.org/10.1063/1.4976972]

I. INTRODUCTION

The nature and mechanism of charge transfer reactions is of interest to a wide range of scientific disciplines. For example, the ability to control charge transfer processes is an important aspect of research on solar cells,[1,2] ion batteries,[3,4] ion sensors,[5,6] and molecular electronics.[7,8] Various charge exchange processes between particles in the universe serve as an important tool for astrophysical research. The emitted photons are used to analyze and identify compositional and flux changes in solar or stellar winds.[9,10]

Only recently experimental techniques have become available allowing the investigation of charge transfer reactions between atoms and ions at ultracold and cold temperatures.[11–18] These novel capabilities have paved the way towards explorations of the fundamental principles of reactivity at the quantum level. Recent theoretical studies[19–30] mostly involve ultracold neutral alkali-metal or alkaline-earth atoms and fairly cold alkaline-earth or rare-earth ions. This selection of atoms and ions has its background in the ready availability of these species in on-going experiments with hybrid atom-ion traps.[11,12,14,16]

Currently, the accuracy of these theoretical studies is limited by uncertainties in the short-range shape of the atom-ion potentials, where the electronic clouds of the atoms significantly overlap. This state of affairs was not unlike that for neutral alkali-metal dimer potentials twenty five years ago when laser cooling was at its infancy. Clear exceptions are systems dealing with light atoms such as hydrogen.[31] In contrast, the long-range description of atom-ion potentials is much better characterized. The leading term is an attractive $-C_4/R^4$ induction potential with a coefficient C_4 that is proportional to the static polarizability of the neutral atom and R is the separation between the two particles.

In parallel, multi-channel quantum-defect theories have been developed that parameterize the short-range atom-ion interactions in terms of boundary conditions for the wavefunctions in conjunction with scattering from the long-range potentials.[32–36] They circumvent the need to explicitly know the short-range potentials by replacing them with a few short-range parameters. Reference 35 observed that as few as three parameters can describe the collisional dynamics over a relatively large range of collisional energies E extending from the ultra-cold regime to about $E/k = 1$ K, where k is the Boltzmann constant.

Atom-ion charge transfer represents one of the simplest, yet still relevant chemical reaction. Broadly speaking, charge transfer of distinct atomic species A and B can be classified by two processes: non-radiative $A + B^+ \rightarrow A^+ + B$ and radiative $A + B^+ \rightarrow A^+ + B + \gamma$ or $A + B^+ \rightarrow AB^+ + \gamma$, where a photon γ is emitted. In the last process, better known as radiative association, vibrationally excited molecular ions are formed. Radiative charge exchange with its spontaneously emitted photon is commonly described with optical potentials.[23,24,37] Stimulated association due to the always-present black-body radiation can enhance the rates.[38]

Several experimental and theoretical groups[11,19,31,35] have investigated charge-exchange collisions between different isotopes of the same atomic species, where the transition is nearly energetically resonant. The rate of such non-radiative processes approaches the Langevin rate.

An intriguing possibility in collisional physics and chemistry is that the reaction can be controlled to achieve or optimize a specific outcome. Precedents for manipulating charge-exchange reaction rates with radiation exist in the literature. Reference 39 proposed to use a photon-induced crossing point between entrance-exit channels that occurs at a short internuclear separation, whereas Refs. 40 and 41 used a crossing point at a large separation. Their predictions for the reaction cross section are based on the Landau-Zener theory of curve crossings. Later studies[42,43] made use of improved computational capabilities to better describe the molecular electronic properties and thus give a better understanding of controlled charge exchange. In addition, laser-induced control of chemical reactions is widely used in chemistry in the thermal regime[44–47] and involves bound-to-continuum transitions in order to break one or more bonds. In the ultracold domain, the control might

involve preparation of the initial reactants as used in Refs. 15, 17, and 48.

In this paper, we explore the control of the charge-exchange reaction at a low temperature by applying laser radiation with a frequency that is nearly resonant to the energy difference between the entrance and exit channels. Here, this implies that we study the continuum-to-continuum transition $A+B^+ + n\gamma \rightarrow A^+ + B + (n+1)\gamma$, where n is the photon number. We demonstrate that this stimulated radiative charge transfer can be enhanced by several orders of magnitude with laser intensities of 10^6 W/cm^2 or larger. We focus on cold charge-exchange collisions between Ca and Yb$^+$ in the presence of linearly polarized radiation with wavenumbers between 400 cm^{-1} and 1200 cm^{-1} and intensities up to 10^{12} W/cm^2. Transitions occur between the excited $A^2\Sigma^+$ and ground $X^2\Sigma^+$ state potentials.

The paper is organized as follows. Section II reviews our *ab initio* adiabatic potential energy surfaces and describes our procedure to diabatize the potentials. These diabatic potentials are then used in Sec. III in a coupled-channels calculation that includes the coupling to the radiation field. Results on the laser intensity, collision energy, and frequency dependence of the reaction rate are given in Sec. IV. We summarize the results in Sec. V.

II. ADIABATIC AND DIABATIC ELECTRONIC POTENTIALS

We, first, determine the non-relativistic ground and excited CaYb$^+$ potentials as a function of internuclear separation R using multi-configuration second-order perturbation theory (CASPT2) implemented in the MOLCAS software suite.[49] Reference wave functions are obtained from a complete active space self consistent field (CASSCF) calculation with 4s4p5s orbitals of Ca and 6s6p7s orbitals of Yb in the active space. This is followed by a CASPT2 calculation, where the $3s^2$ $3p^6$ electrons of Ca and $5s^2$ $5p^6$ $4f^{14}$ electrons of Yb are correlated. Here, the TZVP ANO-RCC (triple-zeta valence polarized atomic natural orbital relativistic CASSCF/CASPT2) basis sets[50] contain (20s 16p 6d 4f) [6s 5p 2d 1f] functions for Ca and (25s 22p 15d 11f 4g 2h) [8s 7p 5d 3f 2g 1h] functions for Yb. The relevant electronic dipole moments and non-adiabatic coupling term between the CaYb$^+$ and Ca$^+$Yb molecular potentials have also been calculated using the CASSCF method.

The two energetically lowest potentials, $V_X(R)$ and $V_A(R)$, for the $^2\Sigma^+$ symmetry are presented in Fig. 1(a). We see that the ground X potential is much deeper than the excited A potential and that they have an avoided crossing at $R_c = 15a_0$ with a splitting of $\Delta V/(hc) = 1000$ cm^{-1}, where h is the Planck constant and c is the speed of light. These potentials dissociate to the atomic Ca$^+$(^{2}S) + Yb(^{1}S) and Ca(^{1}S) + Yb$^+$(^{2}S) limits, respectively. The two limits are split by $\Delta/(hc) = 1136$ cm^{-1}. The potentials have an attractive long-range $-C_4/R^4$ tail, where $C_4 = 71.5E_h a_0^4$ for the X state[51] and $78.5E_h a_0^4$ for the A state.[52] Here E_h is the Hartree energy. Figure 1(b) shows the electronic transition dipole moment $d(R)$ between these $^2\Sigma^+$ states. The transition dipole moment has a maximum at $R = 13a_0$ and approaches zero for large interatomic separations.

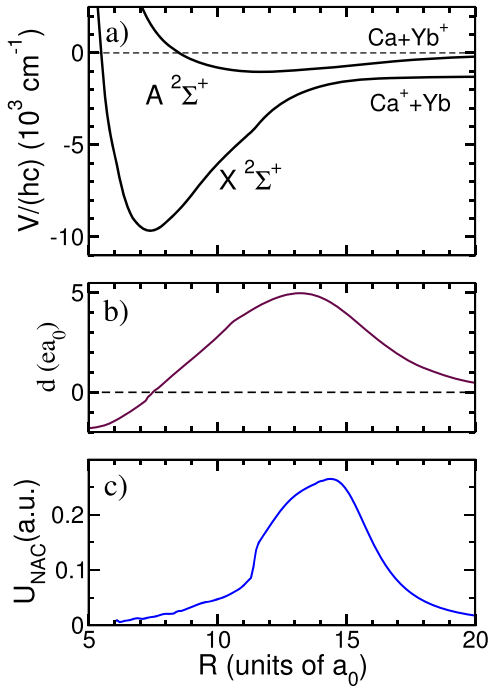

FIG. 1. Electronic properties of the CaYb$^+$ molecule. Panel (a) shows the ground $X^2\Sigma^+$ and excited $A^2\Sigma^+$ adiabatic potential curves as a function of interatomic separation R. Panels (b) and (c) show the transition electric dipole moment and the nonadiabatic coupling term $U_{\rm NAC}(R)$ between these two states as a function of R. For all panels, lengths are expressed in the Bohr radius a_0 = 0.0529 nm and the dipole moment is given in units of ea_0, where e is the charge of the electron.

Other excited state potentials (not shown in Fig. 1(a) lie $\approx$13 000 cm^{-1} above the A potential and do not contribute to the reaction, so that in our computation we can focus on these two lowest electronic potentials.

The corresponding electronic molecular states, denoted by $|X;R\rangle$ and $|A;R\rangle$, parametrically depend on R. Consequently, non-adiabatic coupling between the potentials, proportional to $U_{\rm NAC}(R) = \langle X;R|\, d/dR\, |A;R\rangle$ and shown in Fig. 2(c), leads to non-radiative charge transfer reaction when the collision entrance channel is Ca(^{1}S) + Yb$^+$(^{2}S), the continuum of the A state potential.

In order to set up the closed-coupling calculation, we diabatize the adiabatic X and A potentials by introducing the two diabatic wavefunctions

$$\begin{pmatrix} |1\rangle \\ |2\rangle \end{pmatrix} = O(R) \begin{pmatrix} |X;R\rangle \\ |A;R\rangle \end{pmatrix} \tag{1}$$

with orthogonal transformation

$$O(R) = \begin{pmatrix} \cos(\theta) & \sin(\theta) \\ -\sin(\theta) & \cos(\theta) \end{pmatrix} \tag{2}$$

and angle $\theta(R) = \int_R^\infty U_{\rm NAC}(R')dR'$.

Diabatic states $|1\rangle$ and $|2\rangle$, by *construction* are assumed to be R independent, are coupled according to the 2×2 potential matrix

$$V^{\rm mol}(R) = \begin{pmatrix} V_1(R) & V_{12}(R) \\ V_{12}(R) & V_2(R) \end{pmatrix} = O(R) \begin{pmatrix} V_X(R) & 0 \\ 0 & V_A(R) \end{pmatrix} O^T(R) \tag{3}$$

where $O^T(R)$ is the matrix transpose of $O(R)$. The diabatic potentials $V_1(R)$ and $V_2(R)$ and coupling function $V_{12}(R)$ are

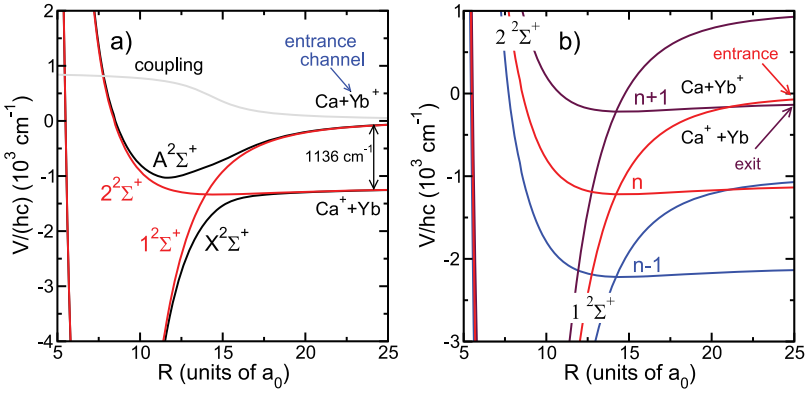

FIG. 2. Panel (a): The ground $X^2\Sigma^+$ and excited $A^2\Sigma^+$ adiabatic (black curves) and the $1^2\Sigma^+$ and $2^2\Sigma^+$ diabatic (red curves) potential energy curves of $CaYb^+$ as a function of R. Only energies near the dissociation limits are shown. Panel (b): Dressed picture of the $CaYb^+$ potentials as a function of R with $n-1$, n, and $n+1$ photons and $\ell = 0$. The photon wavenumber is 1000 cm^{-1}. Here, we assume that the entrance channel corresponds to the potential with n photons that asymptotically has the largest energy.

shown in Fig. 2(a). Similarly, the dipole moment matrix in the diabatic basis set is

$$\begin{pmatrix} D_1(R) & D_{12}(R) \\ D_{12}(R) & D_2(R) \end{pmatrix} = O(R) \begin{pmatrix} d_X(R) & d(R) \\ d(R) & d_A(R) \end{pmatrix} O^T(R), \quad (4)$$

where $d_X(R)$ and $d_A(R)$ are the permanent dipole moments of the X and A states.

III. COUPLED-CHANNELS CALCULATION

We set up a multi-channel description of charge-exchange collisions between an atom and an ion in the presence of near-resonant linearly polarized laser light using the dressed-state picture or the Floquet Ansatz. We construct coupled time-independent radial Schrödinger equations for the interatomic separation R in basis states $|\alpha, m_S; \ell m_\ell; n\rangle = |\alpha, m_S\rangle|\ell m_\ell\rangle|n\rangle$, where $|\alpha, m_S\rangle$ are the diabatic $^2\Sigma^+$ electronic states with $\alpha = 1$ or 2 and $m_S = \pm 1/2$ is the projection quantum number of the electron spin S of the ^{2}S ion along the laser polarization. The ket $|\ell m_\ell\rangle \equiv Y_{\ell m_\ell}(\hat{R})$ is a spherical harmonic describing the relative rotational wavefunction of the two particles around the center of mass with a projection quantum number m_ℓ along the direction of the laser polarization. Finally, $|n\rangle$ is a Fock state with n laser photons of frequency ω.

Figure 2(b) illustrates the dressed states picture of the $CaYb^+$ potentials with $n-1$, n, and $n+1$ photons and $\ell = 0$. The figure shows three pairs of diabatic potential curves shifted by photon energy $\hbar\omega$ with $\hbar = h/(2\pi)$. For the 1000 cm^{-1} laser frequency, used in the figure, an additional crossing near $R = 21a_0$ is created between the entrance channel with n photons and an exit channel with $n+1$ photons. This leads to a new reaction pathway with an exit channel with a small relative kinetic energy between the particles.

The Hamiltonian of our system is

$$H = -\frac{\hbar^2}{2\mu_r}\frac{d^2}{dR^2} + \frac{\mathbf{L}^2}{2\mu_r R^2} + V^{\rm mol}(R) + V^{\rm rad}(\mathbf{R}) + \hbar\omega a^\dagger a, \quad (5)$$

where μ_r is the reduced mass, $\mathbf{L}$ is the rotational angular momentum operator, $|\ell m_\ell\rangle$ are the eigenstates of $\mathbf{L}^2$, and $V^{\rm mol}(R)$ is the electronic Hamiltonian defined in Sec. II. For a $^2\Sigma^+$ system the Hamiltonian $V^{\rm mol}(R)$ is isotropic and does not affect or couple rotational states.

The last two terms in Eq. (5) describe the coupling between the particles and laser field and the Hamiltonian of the field, respectively. In the dipole and long-wavelength approximations, the molecule-field interaction $V^{\rm rad}(\mathbf{R}) = -\sqrt{2\pi\hbar\omega/V}\,(\vec{\epsilon}\cdot\vec{D})(a^\dagger + a)$, where $\vec{D}$ is the molecular electric dipole moment operator, constructed from Eq. (4), and the field operators $a^\dagger$ and a create and destroy laser photons of frequency ω and polarization $\vec{\epsilon}$ in volume V. This molecule-field interaction is anisotropic and only has non-zero matrix elements between states that differ by one photon. We choose the polarization vector $\vec{\epsilon}$ along the laboratory z axis. In our basis, the matrix elements are

$$\langle 1, m_S; \ell m_\ell; n+1|V^{\rm rad}|2, m_S; \ell' m'_\ell; n\rangle = -D_{12}(R)\sqrt{\frac{2\pi I}{c}}\sqrt{\frac{2\ell'+1}{2\ell+1}}C^{\ell m_\ell}_{10,\ell' m'_\ell}C^{\ell 0}_{10,\ell' 0}, \quad (6)$$

where $D_{12}(R) = \langle 1, m_S|d_z|2, m_S\rangle$ is the electronic transition dipole moment for our linearly polarized photon and $I = nc\hbar\omega/V$ is the laser intensity. The functions $C^{jm}_{j_1 m_1 j_2 m_2}$ are Clebsch-Gordan coefficients.

The charge exchange rate coefficient from $|1, m_S\rangle$ with n photons is given by

$$K = \frac{\hbar\pi}{\mu_r k}\sum_{\ell,\ell'=0}^{\ell_{\rm max}}\sum_{m_\ell}\sum_{n'=n-\delta n}^{n+\delta n}|T_{2,\ell' m_\ell, n' \leftarrow 1,\ell, m_\ell, n}|^2, \quad (7)$$

where k is the collisional wave vector, m_ℓ varies from $-\min(\ell, \ell')$ to $\min(\ell, \ell')$, $\delta n = 1$ or 2 in our simulations, and $T_{f\leftarrow i}$ are the T-matrix elements obtained from the scattering solutions of Eq. (5). We find that the main contribution to K comes from T-matrix elements with $n' = n+1$, which corresponds to the transition $|1\rangle + n\hbar\omega \rightarrow |2\rangle + (n+1)\hbar\omega$.

We neglect effects of the permanent dipole moments $D_1(R)$ and $D_2(R)$ as the detuning between states of the same molecular state but with different photon number is large. Moreover, such coupling does not lead to charge exchange.

To calculate the non-radiative and stimulated radiative charge exchange rate, we include many partial waves for both continua. For example, $E/k = 1$ mK and 10 mK requires $\ell_{\rm max} \approx 10$ and 20 partial waves, respectively. In contrast, we only need to include a few partial waves (up to 3 or 4) for collision energies around 1 μK.

IV. RESULTS

We modify the charge-exchange reaction by applying an infra-red laser with frequency near 1000 cm^{-1}. This is a natural choice of the frequency, which is resonant to the adiabatic

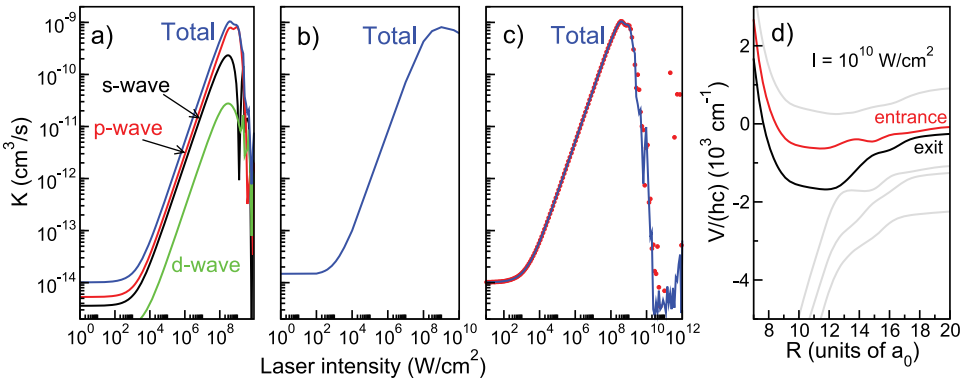

FIG. 3. Charge-exchange rate coefficient for Ca + Yb$^+$ as a function of laser intensity over 10 decades and a laser wavenumber of 1000 cm^{-1}. Panel (a): The collision energy is E/k = 1 μK with one-photon dressing δn = 1. The contribution to the rate of several partial waves is shown by different colored curves. Panel (b): The collision energy is E/k = 1 mK with the same one-photon dressing δn = 1. Panel (c): The total rate coefficient at a collision energy of E/k = 1 μK is shown by a solid blue line for one-photon dressing and by red markers for two-photon dressing. Panel (d): The adiabatic field-dressed potential surfaces that are Stark-shifted and modified by a strong laser field at an intensity of 10^{10} W/cm^2. The laser frequency is 1000 cm^{-1} and E/k = 1 μK.

potential splitting near the avoided crossing at $R = R_c$. Figures 3(a) and 3(b) show the charge-exchange rate coefficient as a function of laser intensity for collision energies of E/k = 1 μK and 1 mK, respectively. In both panels, the intensity is varied over 10 decades, leading to a dramatic change of the rates coefficient.

At low laser intensity, from zero up to 10^2 W/cm^2, the weak non-adiabatic interaction between the adiabatic X and A potentials results in a small reaction rate of the order of 10^{-14} cm^3/s. As the field intensity is increased, from 10^3 to 10^8 W/cm^2, we observe a linear rise in the reaction rate reaching a maximum value close to the Langevin rate for our system. Figure 3(a) also shows the partial wave contribution to the reaction rate coefficient for E/k = 1 μK. Only s, p, and d waves contribute significantly. The calculation becomes more complex for a collision energy of 1 mK in Fig. 3(b) as a greater number of channels are coupled by the laser field. We obtain the total charge-exchange rate coefficient K after summation of the transition matrix elements squared (Eq. (7)) over all possible m_ℓ projections for partial waves from 0 to $\ell_{\max} = 10$. For clarity, contributions from individual partial waves are not shown.

The effect of one- or two-photon dressing (i.e., $\delta n = 1$ or 2) is also studied in Fig. 3(c). The comparison between these two cases demonstrates that the one-photon dressing model is adequate for our hybrid system when the intensity is below 10^{10} W/cm^2. These results are observed for a collision energy of 1 μK. Finally, we note that the total reaction rates in Figs. 3(a) and 3(b) obtained for different collision energies are nearly the same despite of large difference in the contributing number of partial waves.

The strong resonant field creates coupling between the entrance and light-induced exit channels, indicated in Fig. 2(b), and leads to an enhanced reaction rate. Even stronger laser fields with an intensity above 10^9 W/cm^2 modify energies of the interaction potentials inducing a reaction barrier and thereby slowing the reaction. We demonstrate this effect by showing Stark-shifted adiabatic potentials in Fig. 3(d) at $I = 10^{10}$ W/cm^2 and laser frequency of 1000 cm^{-1}.

The total charge-exchange rate coefficient K as a function of collision energy is shown in Fig. 4(a) for several intensities. In the absence of the external field, the rate coefficient is relatively small, only slightly above 10^{-14} cm^3/s, and increases four orders of magnitude when the intensity reaches 10^7 W/cm^2. This occurs uniformly over the 20 mK interval of collision energies shown in the figure. Moreover, the unthermalized rate coefficient has a number of shape resonances due to the many partial waves that contribute. The resonances occur when the energy of the entrance channel matches quasi-bound levels trapped by the long-range potential, $-C_4/R^4 + \hbar^2\ell(\ell+1)/(2\mu_r R^2)$, near the top of the centrifugal barrier. This enhances the wave functions at small separations and thus enhances the charge-exchange rate coefficient. We also find that the resonance positions occur at

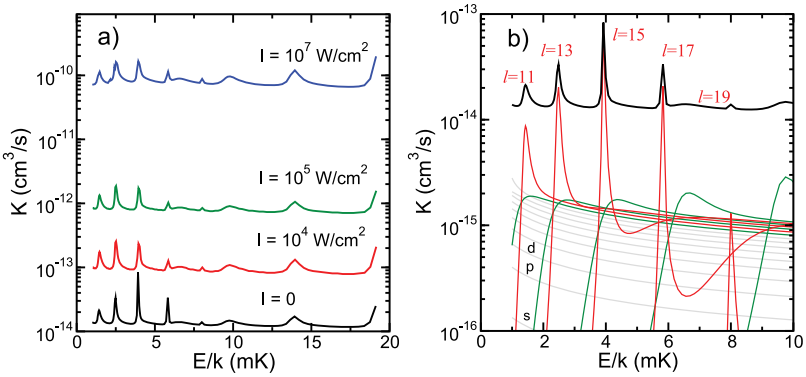

FIG. 4. Panel (a): Charge-exchange rate coefficient for Ca + Yb$^+$ as a function of collision energy E/k from 1 mK to 20 mK for four laser intensities. Panel (b): The partial wave contributions to the rate coefficients at zero intensity. The gray curves correspond to partial rates for $\ell \le 9$, those for s, p, and d waves are indicated in the figure. From left to right the dark-green curves correspond to ℓ = 10, 12, 14, 16, and 18, respectively. Partial rates for ℓ = 11, 13, 15, 17, and 19, shown by red curves, have distinct orbiting resonances. The wavenumber of the laser is 1000 cm^{-1} and δn = 1 in both panels.

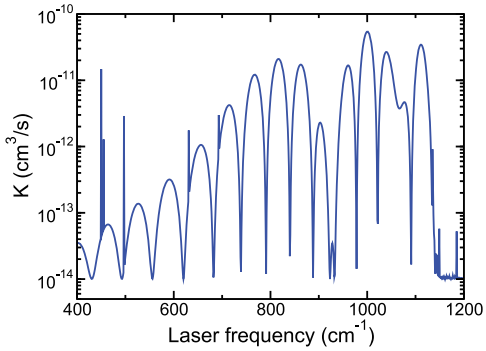

FIG. 5. Charge-exchange rate coefficient for Ca + Yb^+ as a function of laser wavenumber. Laser intensity is 10^7 W/cm^2 and $E/k = 1$ μK.

almost the same collision energy at any laser intensity. There is a slight shift and broadening of the resonances when the intensity is increased. Once we thermalize the rate coefficient, the effect of resonances is less visible.

In our calculations, we are able to identify the partial waves that contribute to the resonances. Figure 4(b) presents plots of partial rate coefficients at zero field intensity for $\ell = 0$–19 as a function of collision energy. For collision energies from 1 mK to 10 mK, resonances occur for odd partial-wave quantum numbers between 11 and 19. Reference 53 showed that the analytical scattering solutions for a $-C_4/R^4$ potential are such that if a shape resonance exists for partial wave ℓ then $\ell + 2, \ell + 4$, etc., resonances also exist. This observation explains our finding that all resonances in Figs. 4(a) and 4(b) are due to odd partial waves.

We also test the dependence of the charge-exchange rate on the laser wavenumber in between 400 cm^{-1} and 1200 cm^{-1}. Figure 5 shows that the rate coefficient is very sensitive to the laser frequency and even oscillates due to changing wave-function overlap at the avoided crossing point between the initial n photon state and the final $n+1$ photon state. The location of this crossing point also changes with the laser frequency. In fact, these are Stueckelberg oscillations. The maximum rate is reached for a wavenumber $\omega/c \approx 1000$ cm^{-1}, which corresponds to the closest approach of the adiabatic potentials. For $\omega/c > 1136$ cm^{-1}, the energy difference between the dissociation limits, the laser light does not affect the charge-exchange rate and leads to K of the order 10^{-14} cm^3/s. The laser-induced crossing between the entrance and exit channels shown in Fig. 2 does not occur any more.

V. SUMMARY

We have explored the effect of a moderately intense laser field on the charge transfer reaction for hybrid atom-ion collisions in the realm of cold temperatures. We have shown that the reaction rate coefficient can be significantly enhanced with a near-resonant laser field. We find that around a field intensity of 10^3 W/cm^2, the reaction mechanism changes from being dominated by the intra-molecular non-adiabatic coupling to being laser field dominated. We investigate these processes over a wide range of laser intensities, laser frequencies, and collision energies.

SUPPLEMENTARY MATERIAL

See supplementary material for the complete electronic structure potential surfaces $X^2\Sigma^+$ and $A^2\Sigma^+$ of $CaYb^+$, as well as transition dipole moment and radial non-adiabatic coupling between these potentials.

ACKNOWLEDGMENTS

This work is supported by Grants of the ARO-MURI Nos. W911NF-14-1-0378 and W911NF-12-1-0476, the NSF No. PHY-1619788.

[1] Y. Liu, Y. Feng, and M. Sun, Sci. Rep. **5**, 13970 (2015).
[2] C. S. Ponseca, Y. Tian, V. Sundström, and I. G. Scheblykin, Nanotechnology **27**, 082001 (2016).
[3] R. Hausbrand, D. Becker, and W. Jaegermann, Prog. Solid State Chem. **42**, 175 (2014).
[4] J. W. Choi and D. Aurbach, Nat. Rev. Mater. **1**, 16013 (2016).
[5] M. Shahinpoor, Electrochim. Acta **48**, 2343 (2003).
[6] B. Cho, M. G. Hahm, M. C. J. Yoon, A. R. Kim, Y.-J. Lee, S.-G. Park, J.-D. Kwon, C. S. Kim, M. Song, Y. Jeong, K.-S. Nam, T. J. Y. S. Lee, C. G. Kang, B. H. Lee, H. C. Ko, P. M. Ajayan, and D.-H. Kim, Sci. Rep. **5**, 8052 (2015).
[7] K. Kawai, H. Kodera, Y. Osakada, and T. Majima, Nat. Chem. **1**, 156 (2009).
[8] E. J. Dell, B. Capozzi, J. Xia, L. Venkataramam, and L. M. Campos, Nat. Chem. **7**, 209 (2015).
[9] R. Lallement, Astron. Astrophys. **422**, 391 (2004).
[10] L. Gu, J. Kaastra, and A. J. J. Raassen, Astron. Astrophys. **588**, A52 (2016).
[11] A. T. Grier, M. Cetina, F. Oručvić, and V. Vuletić, Phys. Rev. Lett. **102**, 223201 (2009).
[12] C. Zipkes, S. Palzer, L. Ratschbacher, C. Sias, and M. Köhl, Phys. Rev. Lett. **105**, 133201 (2010).
[13] S. Schmid, A. Härter, and J. H. Denschlag, Phys. Rev. Lett. **105**, 133202 (2010).
[14] F. H. J. Hall, M. Aymar, N. Bouloufa-Maafa, O. Dulieu, and S. Willitsch, Phys. Rev. Lett. **107**, 243202 (2011).
[15] F. H. J. Hall and S. Willitsch, Phys. Rev. Lett. **109**, 233202 (2012).
[16] W. G. Rellergert, S. T. Sullivan, S. Kotochigova, A. Petrov, K. Chen, S. J. Schowalter, and E. R. Hudson, Phys. Rev. Lett. **107**, 243201 (2011).
[17] L. Ratschbacher, C. Zipkes, C. Sias, and M. Köl, Nat. Phys. **8**, 649 (2012).
[18] S. Haze, R. Saito, M. Fujinaga, and T. Mukaiyama, Phys. Rev. A **91**, 032709 (2015).
[19] R. Coté and A. Dalgarno, Phys. Rev. A **62**, 012709 (2000).
[20] A. Watanabe, C. Dutta, P. Nordlander, M. Kimura, and A. Dalgarno, Phys. Rev. A **66**, 044701 (2002).
[21] L. B. Zhao, P. C. Stancil, J. P. Gu, H. Liebermann, Y. Li, P. Funke, R. J. Buenker, B. Zygelman, M. Kimura, and A. Dalgarno, The Astrophys. J. **615**, 1063 (2004).
[22] P. Zhang, E. Bodo, and A. Dalgarno, J. Phys. Chem. A **113**, 15085 (2009).
[23] C. H. Liu, Y. Z. Qu, Y. Zhou, J. G. Wang, Y. Li, and R. J. Buenker, Phys. Rev. A **79**, 042706 (2009).
[24] X. J. Liu, Y. Z. Qu, B. J. Xiao, C. H. Liu, Y. Zhou, J. G. Wang, and R. J. Buenker, Phys. Rev. A **81**, 022717 (2010).
[25] M. Tacconi, F. A. Gianturco, and A. K. Belyaev, Phys. Chem. Chem. Phys. **13**, 19156 (2011).
[26] P. Zhang, A. Dalgarno, R. Cote, and E. Bodo, Phys. Chem. Chem. Phys. **13**, 19026 (2011).
[27] H. D. L. Lamb, J. F. McCann, B. M. McLaughlin, J. Goold, N. Wells, and I. Lane, Phys. Rev. A **86**, 022716 (2012).
[28] A. K. Belyaevi, S. A. Yakovleva, M. Tacconi, and F. A. Gianturco, Phys. Rev. A **85**, 042716 (2012).
[29] E. R. Sayfutyarova, A. A. Buchachenko, S. A. Yakovleva, and A. K. Belyaev, Phys. Rev. A **87**, 052717 (2013).
[30] B. M. McLaughlin, H. D. L. Lamb, I. Lane, and J. F. McCann, J. Phys. B: At., Mol. Opt. Phys. **47**, 145201 (2014).
[31] E. Bodo, P. Zhang, and A. Dalgarno, New J. Phys. **10**, 033024 (2008).
[32] Z. Idziaszek, T. Calarco, and P. Zoller, Phys. Rev. A **76**, 033409 (2007).
[33] Z. Idziaszek, T. Calarco, P. Julienne, and A. Simoni, Phys. Rev. A **79**, 010702(R) (2009).
[34] Z. Idziaszek, A. Simoni, T. Calarco, and P. S. Julienne, New J. Phys. **13**, 083005 (2011).

[35]M. Li and B. Gao, Phys. Rev. A **86**, 012707 (2012).
[36]B. Gao, Phys. Rev. A **88**, 022701 (2013).
[37]B. Zygelman, A. Dalgarno, M. Kimura, and N. F. Lane, Phys. Rev. A **40**, 2340 (1989).
[38]B. Zygelman, P. C. Stancil, and A. Dalgarno, Astrophys. J. **508**, 151 (1998).
[39]R. Z. Vitlina, A. V. Chaplik, and M. V. Entin, Sov. Phys.-JETP **40**, 829 (1975).
[40]D. A. Copeland and C. L. Tang, J. Chem. Phys. **65**, 3161 (1976).
[41]D. A. Copeland and C. L. Tang, J. Chem. Phys. **66**, 5126 (1977).
[42]Y. P. Hsu, M. Kimura, and R. E. Olson, Phys. Rev. A **31**, 576 (1985).
[43]T.-S. Ho, C. Laughlin, and S.-I. Chu, Phys. Rev. A **32**, 122 (1985).
[44]P. W. Brumer and M. Shapiro, *Optical Control of Molecular Dynamics* (Wiley-Interscience, Hoboken, NY, 2000).
[45]S. A. Rice and M. Zhao, *Principles of the Quantum Control of Molecular Processes* (Wiley, NY, 2003).
[46]A. D. Bandrauk, *Molecules in Laser Fields* (Marcel Dekker, New York, 1994).
[47]B. J. Sussman, D. Townsend, M. Y. Ivanov, and A. Stolow, Science **314**, 278 (2006).
[48]S. T. Sullivan, W. G. Rellergert, S. Kotochigova, and E. R. Hudson, Phys. Rev. Lett. **109**, 223002 (2012).
[49]G. Karlström, R. Lindh, P.-A. Malmqvist, B. O. Roos, U. Ryde, V. Veryazov, P.-O. Widmark, M. Cossi, B. Schimmelpfennig, P. Neogrady, and L. Seijo, in *Proceedings of the Symposium on Software Development for Process and Materials Design* [Comput. Mater. Sci. **28**, 222 (2003)].
[50] See http://molcas.org/ for Molcas 7.
[51]P. Zhang and A. Dalgarno, J. Phys. Chem. A **111**, 12471 (2007).
[52]S. Porsev and A. Derevianko, J. Exp. Theor. Phys. **102**, 195 (2006).
[53]B. Gao, Phys. Rev. Lett. **104**, 213201 (2010).